Article:
Jin, H., Ghazizadeh, S. and Provis, J.L. orcid.org/0000-0003-3372-8922 (2023) Assessment of the thermodynamics of Na,K-shlykovite as potential alkali-silica reaction products in the (Na,K)2O-CaO–SiO2-H2O system. Cement and Concrete Research, 172. 107253. ISSN: 0008-8846

https://doi.org/10.1016/j.cemconres.2023.107253

Cement and Concrete Research 172 (2023) 107253

Contents lists available at ScienceDirect

Cement and Concrete Research

journal homepage: www.elsevier.com/locate/cemconres

Assessment of the thermodynamics of Na,K-shlykovite as potential alkali-silica reaction products in the $(Na,K)_2O$-CaO–SiO_2-H_2O system

Haoliang Jin [a], Sam Ghazizadeh [b], John L. Provis [a,*]

[a] Department of Materials Science and Engineering, The University of Sheffield, United Kingdom
[b] Special Services, Mott MacDonald, London, United Kingdom

ARTICLE INFO

Keywords:
Alkali-silica reaction
Thermodynamic modelling
Phase diagrams

ABSTRACT

The thermodynamic description of the alkali-silica reaction is incomplete, due to the lack of thermodynamic data for the alkali-silica reaction products. Here, we estimate the temperature-dependent thermodynamic properties of Na- or K-shlykovite phases which are found to form during alkali-silica reaction in concrete. The thermodynamic properties are then used to produce a series of binary phase diagrams considering different concentrations of alkalis. The results show that these two products start to form at 0.01 mol/kg of alkalis in the CaO–SiO_2 binary phase diagrams. Both Na- and K-shlykovite can co-exist with C-S-H at an increased concentration of CaO, consistent with findings that these alkali-silica reaction products may form in real cement systems. However, there is a maximum alkali concentration in the binary phase diagram beyond which shlykovite cannot form, due to limited calcium solubility. This work can help understand and improve alkali-silica testing protocols proposed in standards.

1. Introduction

One of the most important factors that restrict the development of research into alkali-silica reaction (ASR) in concretes is the lack of understanding and observation of the ASR products. The relatively minute amount of ASR products, which form a small fraction of the total concrete mass and typically develop near the interfacial transition zone and within aggregates, requires the use of high resolution and spatially-resolved tools to properly observe and characterise [1]. Additionally, when ASR products are investigated, they are sometimes difficult to distinguish from calcium silicate hydrates (C-S-H) due to their similar chemical compositions [2]. Recently, advanced analytical techniques such as Raman microscopy [3–5], in-situ synchrotron-based micro-X-ray diffraction [6], and micro X-ray absorption spectroscopy (XAS) [7] have been used to observe the characteristics of ASR products, and have shown that amorphous ASR products form in cracks within aggregates at the early stage, but then transform into crystalline products as the reaction progresses further [5].

The reaction between alkali (sourced largely but not solely from cement paste) and silicate from reactive aggregates forms ASR products. Calcium ions from the cement also take part in the reaction, alongside the alkali ions, as the reaction proceeds over time. The average atomic ratios Ca/Si and (Na + K)/Si of ASR products have been measured to be 0.21–0.23 and 0.21–0.34, respectively, regardless of the amorphous or crystalline nature of the structures [5,8–10]. Raman microscopy results have revealed that the ASR products exhibit a layered silicate framework, with cations such as sodium and/or potassium, as well as water, filling the interlayer spaces [11]. To better understand the structure of ASR products and their expansion mechanism, natural minerals such as okenite ($CaSi_2O_5{\cdot}2H_2O$) [12], mountainite ($KNa_2Ca_2[Si_8O_{19}(OH)]{\cdot}6H_2O$) [13] and rhodesite ($KHCa_2[Si_8O_{19}]{\cdot}5H_2O$) [14] are often used as natural analogues to compare with crystalline ASR products. Shi et al. [15] have successfully synthesized two shlykovite-group minerals ($KCaSi_4O_8(OH)_3{\cdot}2H_2O$ and $NaCaSi_4O_8(OH)_3{\cdot}2.3H_2O$) in the laboratory where sodium substitutes for potassium in the layered structure and with slightly different interlayer water contents (see Appendix, Table A1). These minerals are considered to closely resemble some of the ASR products observed in the field [16].

Thermodynamic modelling is a mature way to predict phase assemblages in cement systems, based on the principle of Gibbs energy minimisation with mass balance constraints. The increasing completeness of the databases of minerals and other phases relevant to cement and concrete science are now allowing this approach to be considered as an efficient method to predict durability-oriented performance of

* Corresponding author.
E-mail addresses: hjin15@sheffield.ac.uk (H. Jin), sam.ghazizadeh@mottmac.com (S. Ghazizadeh), j.provis@sheffield.ac.uk (J.L. Provis).

https://doi.org/10.1016/j.cemconres.2023.107253
Received 10 October 2022; Received in revised form 6 June 2023; Accepted 4 July 2023
Available online 6 July 2023

concrete under different exposure environments, and to complement the established experimental approaches. This is particularly crucial for ASR which is a slow process and for which standard testing methods struggle to reliably assess all types of cement and aggregate combinations under realistic conditions.

Previous publications on ASR processes have primarily focused on investigating the dissolution of silica and conducting pertinent theoretical calculations [17,18]. As more natural minerals that are like ASR products are identified and the database further constructed, the modelling results can better reflect and explain the formation of ASR products. For example, Kim and Olek [19] considered the role of OH^- in the pore solution in the process of the dissolution of reactive silica, using kanemite ($KHSi_2O_5{\cdot}3H_2O$ or $NaHSi_2O_5{\cdot}3H_2O$) as model ASR products. Guthrie and Carey [20] provided a model to investigate the effect of pH gradients on the dissolution of silica and ASR precipitation. In their modelling, magadiite [$Na_2Si_7O_3(OH){\cdot}3H_2O$], and okenite [$CaSi_2O_5{\cdot}2H_2O$] were used to simulate low-calcium and high-calcium crystalline ASR products respectively. It is also valuable to enrich the understanding that can be gained from experimental data by using thermodynamic modelling, especially where $Ca(OH)_2$ controls the ASR process [21].

However, the fact that some key structural aspects of these minerals do not correspond fully to the best available understanding of ASR products leads to the suggestion that kanemite- and okenite-type gels may no longer be the most suitable comparators for modelling of field-observed ASR products [1,4,22]. Shi et al. [15] did model the formation of synthetic shlykovite-type products at 80 °C and compared them with their experimental data, which proved the efficacy of thermodynamic modelling for these particular ASR product analogues. However, it is worth noting that these previous studies applied average logK values in their thermodynamic calculations and estimated the pH values, which may impact the accuracy of the modelling results. Also, a key remaining challenge is the incomplete thermodynamic database for shlykovite-type ASR products at 25 °C, which is required to underpin accurate modelling for ASR without thermal acceleration.

The aim of this paper is therefore to build up the thermodynamic parameters of two shlykovite-type ASR products, namely K-shlykovite ($KCaSi_4O_8(OH)_3{\cdot}2H_2O$) and Na-shlykovite ($NaCaSi_4O_8(OH)_3{\cdot}2.3H_2O$), at ambient temperature. Binary phase diagrams with different concentration of alkalis are prepared to verify the reliability of the calculated parameters in conjunction with the established CEMDATA database, by comparison with published experimental data. The general approach adopted in this paper can potentially provide a simple method to build up thermodynamic parameters for other ASR products. The phase diagrams show a foundation for further understanding and predicting phase assemblages for certain combinations of ion concentrations at ambient and higher temperatures. The modelling results can also provide some constructive suggestions for standardising ASR testing.

2. Methods

2.1. Software and database

Modelling in this study is performed using the Gibbs energy minimisation software GEM-Selektor v.3 (http://gems.web.psi.ch/GEMS3/). The Cemdata18.1 cement thermodynamic database [23] is used in this paper; see Appendix, Table A2. At ambient temperature the formation of quartz is quite slow, and thus this phase is excluded from the modelling calculations. The CSHQ solid solution model included in CEMDATA18.1 is used to represent C-S-H with varying Ca/Si ratios.

The activity coefficients of aqueous species are calculated by the Truesdell-Jones form of the extended Debye-Hückel equation, which is shown in Eq. (1):

$$log_{10}\gamma_i = \frac{-A_\gamma z_i^2\sqrt{I}}{1+aB_\gamma\sqrt{I}} + b_\gamma I \quad (1)$$

where the coefficients A_γ and B_γ are related to the temperature and pressure of the system, z_i is the charge of species i, and I is the effective molal ionic strength, which is calculated by Eq. (2):

$$I = \frac{1}{2}\sum_{i=1}^{n} c_i z_i^2 \quad (2)$$

where c_i is the concentration of the i^{th} ionic species. In Eq. (1), a and b_γ are solution-dependent parameters. When NaOH solution is the main aqueous phase, a and b_γ are equal to 3.31 Å and 0.098 kg/mol; these become 3.67 Å and 0.123 kg/mol respectively in KOH-dominated solutions [23].

2.2. Thermodynamic parameter estimation for ASR products

In this study, K-shlykovite ($KCaSi_4O_8(OH)_3{\cdot}2H_2O$) and Na-shlykovite ($NaCaSi_4O_8(OH)_3{\cdot}2.3H_2O$) are considered as representative potential ASR products and used to build up thermodynamic parameters, although there are some variations mentioned in the literature regarding the precise nature of the ASR products that form in real cements [5,22,24]. The factors controlling the structures and the formation of different types of ASR products (in terms of their relationship to different model minerals) are poorly understood and may involve both kinetic and thermodynamic issues. These factors are very difficult to probe experimentally, involving long experiment durations, and further work in this area is ongoing in many laboratories.

For solid hydrates, standard molar entropy and molar heat capacity (where these have not been determined experimentally) are correlated with the formula unit volume V_m, and can be calculated by Eq. (3) (from Eq. (6) in ref. [25]) and Eq. (4) (from Fig. 2 of ref. [26]) respectively:

$$S^\circ = 1579{\cdot}V_m + 6 \quad (3)$$

$$Cp^\circ = 1388.1{\cdot}V_m + 4.58 \quad (4)$$

Gibbs free energies of formation for different ASR products are obtained according to Eq. (5),

$$\Delta_r G^\circ = \sum_i \nu_i \Delta_f G^\circ = -RTlnK \quad (5)$$

where $\Delta_r G^\circ$ is the Gibbs free energy of reaction, which is equal to the sum of Gibbs free energy of formation ($\Delta_f G^\circ$) of each species multiplied by their corresponding stoichiometric coefficients (ν_i, defined to be negative for reactants and positive for products). R is the universal gas constant which is equal to 8.31451 J/mol•K, T is the temperature in Kelvin, and K is the solubility product constant associated with the reference reaction. In this case, the solubility products of the two ASR products are based on Eqs. (6) and (7), respectively [22].

$$K-shlykovite: KCaSi_4O_8(OH)_3{\cdot}2H_2O = K^+ + Ca^{2+} + 4SiO_2 + 3OH^- + 2H_2O \quad K_{s1} \quad (6)$$

$$Na-shlykovite: NaCaSi_4O_8(OH)_3{\cdot}2.3H_2O = Na^+ + Ca^{2+} + 4SiO_2 + 3OH^- + 2.3H_2O \quad K_{s2} \quad (7)$$

In ref. [22], the available solubility products are obtained at 80 °C ($\log_{10} K_{s1} = -25.8 \pm 2$, $\log_{10} K_{s2} = -26.5 \pm 2$). However, all parameters need to be converted to a reference temperature of 25 °C for use in standard Gibbs free energy calculations. Therefore, Eq. (8), with parameters defined by Eqs. (9)–(11), is used to obtain a temperature-dependent log K_T:

$$logK_T = A_0 + A_2T^{-1} + A_3lnT \quad (8)$$

$$A_0 = \frac{0.4343}{R} \bullet \left[\Delta_r S^0_{T_0} - \Delta_r Cp^0_{T_0}(1+lnT_0)\right] \quad (9)$$

$$A_2 = \frac{0.4343}{R} \bullet \left(\Delta_r H^0_{T_0} - \Delta_r Cp^0_{T_0} T_0\right) \quad (10)$$

$$A_3 = \frac{0.4343}{R} \bullet \Delta_r Cp^0_{T_0} \quad (11)$$

where A_0, A_2, A_3 are empirical coefficients, T_0 is 298.15 K (25 °C), and T is the calculation temperature of interest. The quantities $\Delta_r S^0_{T_0}$, $\Delta_r Cp^0_{T_0}$ and $\Delta_r H^0_{T_0}$ are molar entropy, heat capacity, and enthalpy of reaction at T_0, which are calculated from an equation taking the form of Eq. (12) for each quantity; Eq. (12) is defined in terms of a dummy quantity Φ to maintain generality.

$$\Phi_r = \sum_j \nu_j \Phi_{f_j} - \sum_i \nu_i \Phi_{f_i} \quad (12)$$

where Φ_r is either molar entropy, heat capacity, or enthalpy of reaction, while Φ_f is the corresponding parameter of formation; i and j donate reactants and products respectively, and the ν values are the stoichiometric coefficients according to the reference reaction. However, for molar enthalpy of reaction calculations, the standard molar enthalpy of formation for each ASR product is unknown. Therefore, this value may be estimated and fitted iteratively; log K_T can be obtained by keeping changing T in Eq. (8) from 298.15 K to 353.15 K, terminating when the calculated solubility product at 80 °C matches the data from ref. [22].

3. Results and discussion

3.1. Discussion and refinement of errors associated with the solubility products of two ASR products

The term solubility product is used to refer to the product of the activities (or often, but less precisely, the concentrations) of dissolved ions at equilibrium with the solid phase of interest, at a certain temperature. In the calculation of the solubility product of shlykovite-type phases in ref. [22], the hydroxyl ion activity was obtained from pH measurement at about 23 °C, while the concentrations of other ions were gained from ion chromatography analysis for solutions equilibrated at 80 °C. The pH value in that study was simply corrected by 1.47 units to represent the decrease of pH value from 23 °C to 80 °C. In fact, this decrease becomes more complex when involving more ions in the solution, which introduces added uncertainty in the calculation method used in [22], and merits further assessment.

Here, we iteratively refined experimental pH values by a series of temperature-dependent simulations using GEMS, and we use the new values to estimate the solubility product at 80 °C and fit it to 25 °C, as shown in Fig. 1. The black line represents data from [22] while the red line is the recalculation of results in this study. The pH values show a smaller decrease when increasing temperature from 25 °C to 80 °C, compared with the estimates from [22], which means that the solubility products obtained using the new pH value become smaller. In addition, the error bars associated with the solubility products in ref. [22] (±2 units) were stated to have been "roughly estimated" due to the difficulty in generating pure synthesized ASR products. Here we refined all solubility products at 80 °C calculated in Tables 4 and 5 in ref. [22] using the improved pH calculation protocol, and fitting iteratively to determine both the largest and smallest $\log_{10}K$ values that could be consistent with the available data, smaller error bounds can be obtained (±0.4 log units for Na-shlykovite and ± 1.2 for K-shlykovite).

For comparison, if we consider an estimated 10 % analytical uncertainty per aqueous compositional determination (for all components except H_2O and OH^-, both of which can be determined with much higher analytical precision in the pH range of interest and so are not relevant to the error calculation), and propagate this through the solubility product expressions: the sum of the exponents (stoichiometric coefficients) of K (or Na), Ca, and SiO_2 is in each case 6. So, the lower error bound can be estimated as a factor of $(0.9)^6$, and the upper bound as $(1.1)^6$, which gives a range of factors of 0.53 to 1.77. In log units, these become (−0.248 / +0.275) as the error bound contributions in $\log_{10}K$ from the (estimated) analytical uncertainties, which are consistent with the discussion above.

Nonetheless, further experimental studies are necessary to validate the estimated/calculated parameters. Our intention here is to build up a method to develop the thermodynamic parameters of potential ASR products when these are difficult to measure experimentally, and to use them to achieve improved thermodynamic modelling of ASR processes. In this case, Table 1 summarises the resulting thermodynamic parameters for the two potential ASR products at 25 °C.

3.2. Thermodynamic modelling results

In this section, thermodynamic parameters of ASR products will be used to predict phase assemblages in the CaO–SiO_2-H_2O system with or

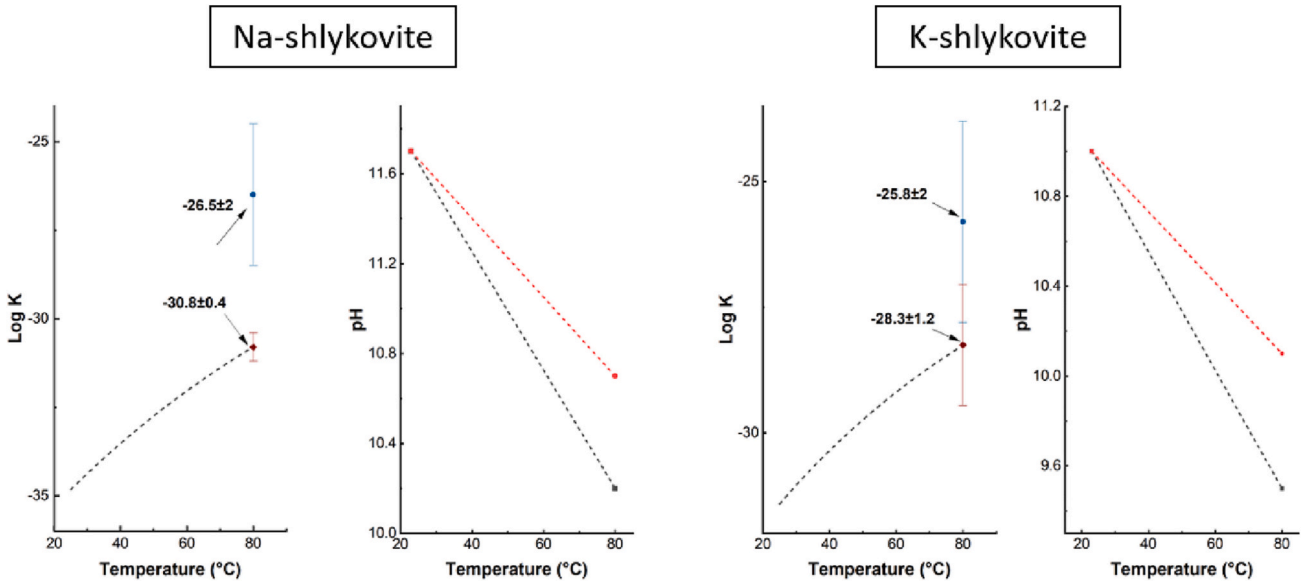

Fig. 1. Refinement and estimation of solubility products of two ASR products at 25 °C by recalculating the pH value (black line: data from ref. [22], red line: calculations in the current study). (For interpretation of the references to colour in this figure legend, the reader is referred to the web version of this article.)

Table 1
Thermodynamic properties for ASR products at 25 °C.

Products	V° (cm^3/mol)	V_m (nm^3·formula-$unit^{-1}$)	$\Delta_f H°$ (kJ/mol)[a]	$\Delta_f G°$ (kJ/mol)[a]	S° (J/mol·K)[a]	Cp° (J/mol·K)[a]	$\log_{10}K$ at 25 °C
K-shlykovite: $KCaSi_4O_8(OH)_3{\cdot}2H_2O$	183	0.3	−5736.4 ± 13	−5293.1 ± 3	485.8 ± 48	426.4 ± 42	−31.2 ± 1.2
Na-shlykovite: $NaCaSi_4O_8(OH)_3{\cdot}2.3H_2O$	164	0.27	−5839.8 ± 15	−5364.4 ± 2	435.9 ± 43	382.5 ± 38	−34.8 ± 0.4

[a] The uncertainties in entropy and heat capacity here were estimated to be ±10 %, which were propagated also to give the uncertainties in enthalpy and Gibbs free energy.

without added alkali oxides, coupled with other potential hydration products. It is worth noting that although error does exist, as mentioned in Section 3.1, the effect of error on each phase diagram will also be discussed in this section.

3.2.1. Binary phase diagram without alkali ions

The CaO-SiO_2 binary phase diagram obtained by thermodynamic modelling is shown in Fig. 2a, which is similar to Fig. 2b, plotted from experimental data and reproduced from [27]. The lines represent the solubility curves of each phase. There are many similarities between the two phase diagrams, including three phases formed, a clear solubility boundary between solution and phases, and phase formation regions. It is important to note that amorphous silica was used instead of quartz in the modelling, thus the solubility product of amorphous silica should correspond to point B in Fig. 2b. However, there still exist some differences here. The main difference is the solubility boundary between C-S-H and the region with amorphous silica plus C-S-H (dashed line), which is a straight vertical line in Fig. 2a, but sloping in Fig. 2b. This is indicating that the Ca^{2+} concentration at which C-S-H is predicted to form in the presence of excess silica is relatively insensitive to the silica concentration, and this may be related to challenges in describing the speciation of polynuclear silicate species in this thermodynamic database [22]. Obviously, without alkali ions there is no ASR product found in the CaO-SiO_2 binary phase diagram, but it is useful to simulate this system to validate the underlying model and to provide a point of comparison for the alkali-containing systems.

3.2.2. Binary phase diagram with addition of a low content of alkalis

The CaO-SiO_2 binary phase diagram with 0.01 mol Na_2O/kg H_2O is shown in Fig. 3a. Note that the units used throughout the paper are molal; "mol/kg" henceforth refers to moles of solute per kg of water. Compared with the unmodified CaO-SiO_2 binary phase diagram, there exist many differences although the basic layout is similar. Firstly, Na-shlykovite is found in all ranges of concentration of SiO_2 because of the presence of Na; regions that form this ASR product occupy partly areas that was solution or formed C-S-H, and the area that corresponded to amorphous silica in the absence of Na has disappeared. This indicates that amorphous silica reacts with Na^+ and CaO to form ASR products instead of C-S-H; the ASR product forms at slightly lower concentrations of SiO_2 and CaO compared with Fig. 1a. It can also be seen that the ASR product can co-exist with C-S-H, which indicates that with an increased concentration of CaO, Na has been partially consumed via the formation of ASR product, while the rest of the Ca continues to react with amorphous silica to form C-S-H. The influence of ASR product and C-S-H formation on aqueous chemistry in these simulations will be explored in more detail in Section 3.4 below.

Another significant difference, when comparing Figs. 3a and 2a (i.e. with and without added Na), can be seen in the position of the solubility boundaries. For example, the solubility of $Ca(OH)_2$ (defined here as the concentration of aqueous Ca^{2+} that exists at the phase boundary where $Ca(OH)_2$ begins to precipitate) also changes from about 0.03 mol/kg (Fig. 2a) to 0.02 mol/kg (Fig. 3) when Na is added.

Replacing K_2O by Na_2O in the thermodynamic modelling, to reflect the importance of potassium in some Portland cements, yields the phase diagram with 0.01 mol/kg of K_2O as shown in Fig. 3b. This phase diagram is evidently similar to the phase diagram with 0.01 mol/kg of Na_2O in the Fig. 3a; the most notable difference is the area at which the ASR product alone forms. It can be seen from Fig. 3b that the area representing the formation of K-shlykovite is smaller than for Na-shlykovite. In other words, K-shlykovite formation commences at a higher concentration of SiO_2, consistent with its less negative solubility product as presented in Section 2.2. In addition, forming K-shlykovite at higher concentrations of SiO_2 leads to a raising of the boundary between the C-S-H single-phase region and the region in which C-S-H coexists with K-

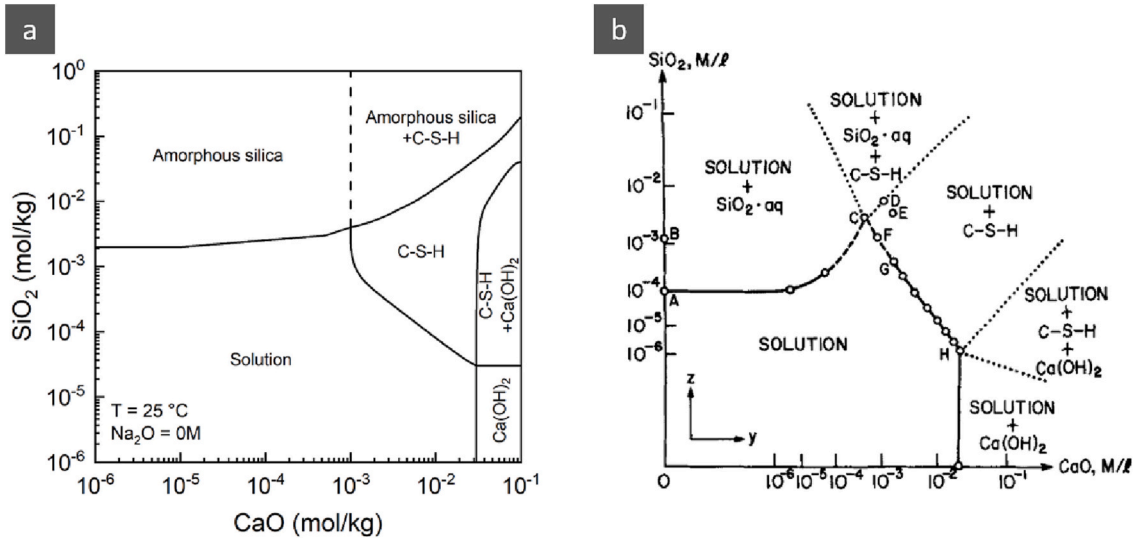

Fig. 2. The CaO-SiO_2 binary phase diagram, (a): obtained by modelling in this study using the GEMS software; (b): experimental data, reproduced by permission from ref. [27], copyright John Wiley & Sons. Note the difference in axis scaling; (a) uses a logarithmic scale for molal concentrations, while (b) is scaled to the 10th root of molar concentrations.

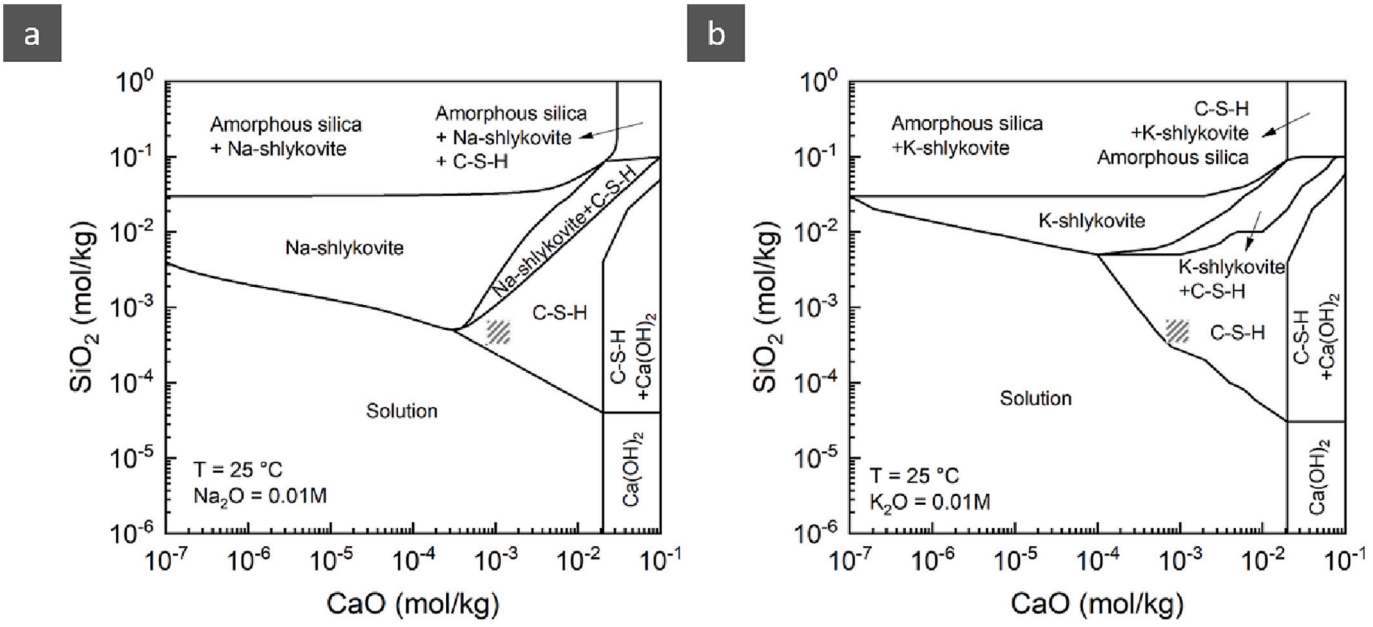

Fig. 3. The CaO-SiO_2 binary phase diagram with 0.01 mol alkalis/kg H_2O: a: Na_2O, b: K_2O. The shaded region represents the approximate dissolved Ca and Si concentrations in the pore fluid of hydrated Portland cement, showing that the simulation accurately predicts this pore fluid to be saturated or slightly supersaturated with respect to C-S-H formation.

shlykovite, compared with that shown in Fig. 3a for the Na-bearing case.

In terms of the effect of error on the phase diagram, phase formation does not change with the change of solubility product. The only difference is the area representing the formation of ASR products, regardless of whether Na or K is the dominant alkali. The ASR products area in the phase diagram becomes larger if a larger solubility product (within the known error bounds) is used in the model, and vice versa.

3.2.3. *The effects of concentration of alkali ions*

To present the effects of concentration of alkali ions on the formation of ASR products and other phases, Fig. 4 shows the effect of varying the amount of alkalis in the simulation from 0.01 mol/kg to 2 mol/kg, at a fixed content of 0.01 mol/kg of CaO. The reason for selecting 0.01 mol/kg of CaO is that the majority of phases formed across system of interest may potentially be present at this CaO concentration (at different concentrations of alkalis and silica) as shown in Fig. 3a. Fig. 4a then highlights that when increasing the concentration of Na_2O from 0.01 mol/kg to 0.03 mol/kg, $Ca(OH)_2$ remains undersaturated, so the bottom left corner of Fig. 4a only contains solution. After that, the addition of extra hydroxide along with the Na^+ moves the solubility curve of $Ca(OH)_2$ to lower concentrations due to the common ion effect, thus $Ca(OH)_2$ starts to form when adding more Na_2O [27]. In terms of C-S-H formation, as can be seen in both Fig. 3a and Fig. 4a, this phase is predicted to be formed even at low concentrations of CaO, and hence the solubility curve that represents the formation of C-S-H begins at the x-axis in Fig. 4a.

Na-shlykovite also forms in Fig. 4a, from 0.01 mol/kg addition of Na_2O and upwards. The areas containing this ASR product are divided into three parts: one where this phase co-exists with C-S-H, while in the other it is present along with amorphous silica due to the depletion of

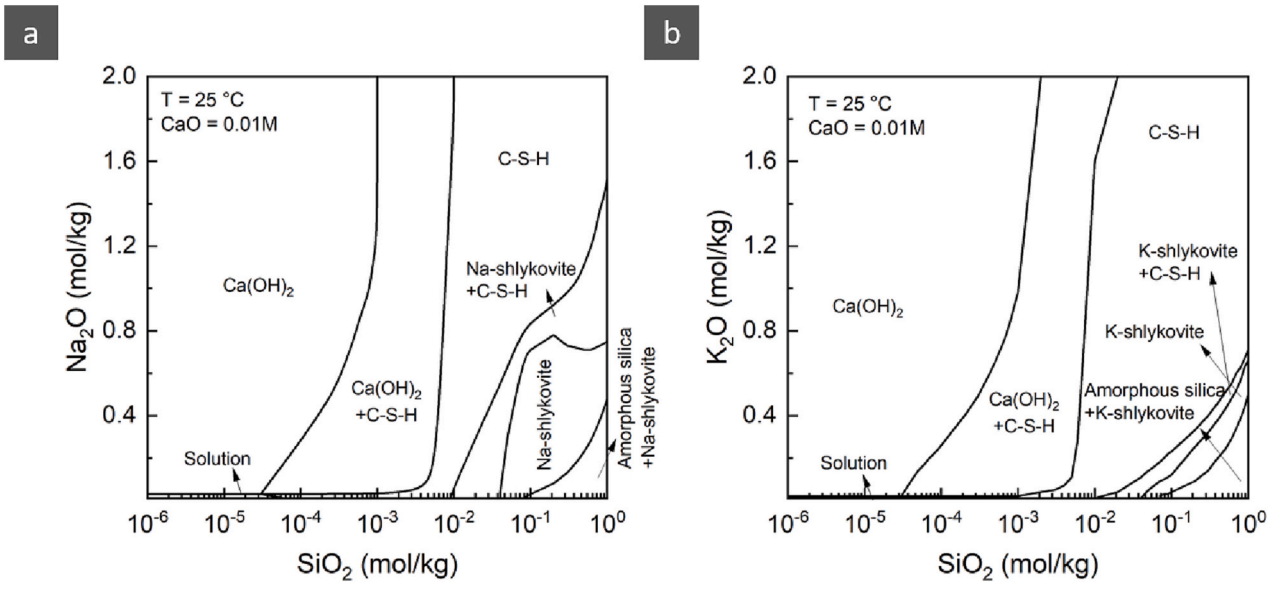

Fig. 4. The alkali-SiO_2 binary phase diagram with fixed 0.01 mol/kg of CaO: a: Na_2O, b: K_2O.

calcium. Between them is the Na-shlykovite single-phase region. The former of these regions is more likely to be achieved in Portland cement-based materials as there is likely to be enough portlandite in the hydrated cement to prevent full calcium depletion. These results are in accordance with the trends shown in Fig. 3a, and the aqueous chemistry will be further discussed in Section 3.4. With a rise in the concentration of SiO_2, more Na is likely to react with the dissolved silica to form ASR products. However, it does not necessarily mean that adding more Na will lead to the formation of more Na-shlykovite; rather, there is a maximum concentration of Na_2O for the formation of Na-shlykovite. Below 1.48 mol/kg of Na_2O, the existence of shlykovite-type ASR products shows the possibility of alkali-silica reactions resulting in this phase. However, above 1.48 mol/kg of Na_2O, this type of ASR product is no longer predicted to form, due to the suppression of calcium solubility. This finding is potentially of interest in the discussion of higher-alkalinity cementitious binders such as alkali-activated cements, for which further insight into the mechanisms of ASR reaction processes is very much needed [28]. Although the temperature of the modelling conducted in this work is different from that used in ref. [29], the results are consistent in showing that at higher Ca/Si ratio and higher alkali contents, C-S-H instead of the ASR product is more stable.

Likewise, the K_2O-SiO_2 binary phase diagram with 0.01 mol/kg of CaO is shown in Fig. 4b. In general, it shows similar trends to the Na_2O-SiO_2 phase diagram, other than a slight difference in the ASR product area. In the presence of K, the threshold for the formation of K-shlykovite reduces to 0.71 mol/kg of K_2O compared with the Na-bearing case. This seems to be consistent with the logK value calculation. The smaller area representing K-shlykovite indicates that it is less favourable to form this product than Na-shlykovite under comparable conditions.

The findings here are not strongly influenced by the uncertainty in solubility products; there exists a threshold for the formation of ASR products. The areas representing the rest of the phases remain unchanged.

3.3. The effect of temperature on the phase diagram

The Na_2O-SiO_2 phase diagrams with 0.01 mol/kg of CaO, at three different temperatures, are shown in Fig. 5; the three temperatures

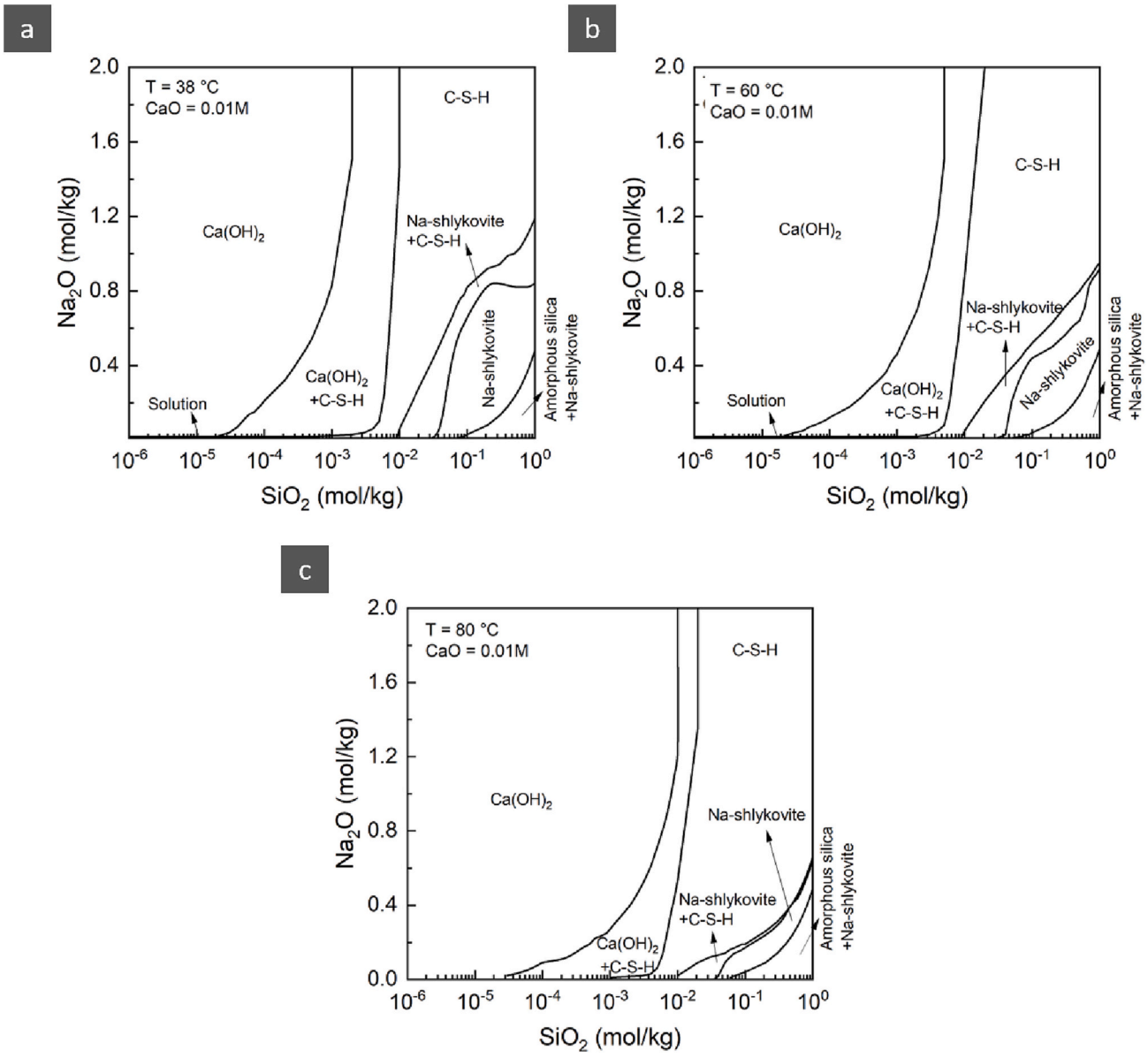

Fig. 5. a: The Na_2O-SiO_2 binary phase diagram with fixed 0.01 mol/kg of CaO at 38 °C; b: the Na_2O-SiO_2 binary phase diagram with fixed 0.01 mol/kg of CaO at 60 °C; c: the Na_2O-SiO_2 binary phase diagram with fixed 0.01 mol/kg of CaO at 80 °C.

shown are selected because these are commonly used in different testing methods that are applied in the laboratory for prediction of ASR. Compared with each other, they have similar areas containing each of the combinations of reaction products, and there are no changes in the phases identified overall. One key difference is that the solution region at very low Na_2O content disappeared at the higher temperatures, instead becoming a $Ca(OH)_2$ area. This is consistent with the well-known retrograde solubility of $Ca(OH)_2$, which means that it forms more readily at higher temperature. There is also some temperature dependence in the Na_2O concentration above which the ASR product disappears. From 38 °C to 80 °C, this phase boundary (at 1 mol/kg of SiO_2) reduced from 1.16 mol/kg to 0.62 mol/kg, and correspondingly also decreased at lower SiO_2 contents. This information might indicate that it is worthwhile to consider to modify ASR testing to use lower concentrations of alkali at higher temperature, to avoid false-negative results caused by suppression of ASR product formation at very high alkalinity, especially for quick testing at higher temperatures.

3.4. Solution chemistry

In order to check and further explain the modelling results, selected regions of the phase diagrams were also analysed in more detail with regard to aqueous chemistry, to calculate the amounts of Na, Ca, Si, and OH^- in the aqueous phase in each case. Because the results presented above for K_2O and Na_2O systems are similar, this analysis is focused solely on the Na_2O-SiO_2 system.

Fig. 6 shows the concentrations of the main components in the solution phase when adding different concentrations of CaO with fixed 0.01 mol/kg of SiO_2, and 0.01 mol/kg of Na_2O. It is worth noting that the concentration of dissolved Ca reduces at 2×10^{-7} mol/kg of CaO, which is due to the formation of more Na-shlykovite with increasing concentration of CaO, as shown in Fig. 3a. After that, the concentration of Ca remains constant due to the formation of this ASR product until 10^{-3} mol/kg of CaO is added, where the rest of Ca stays in the solution because of depletion of the Na_2O added, which leads to an increase in the amount of Ca required to retain saturation with respect to Na-shlykovite. This trend changes at 2×10^{-3} mol/kg of CaO where C-S-H begins to co-exist with the ASR product, as no further Na-shlykovite can form. Then, dissolved Ca tends to decrease in the C-S-H single-phase region. The trend increases again until $Ca(OH)_2$ forms, as shown in Fig. 3a. The concentration of OH^- is directly interrelated with the amount of Ca staying in the solution, thus shows a similar trend.

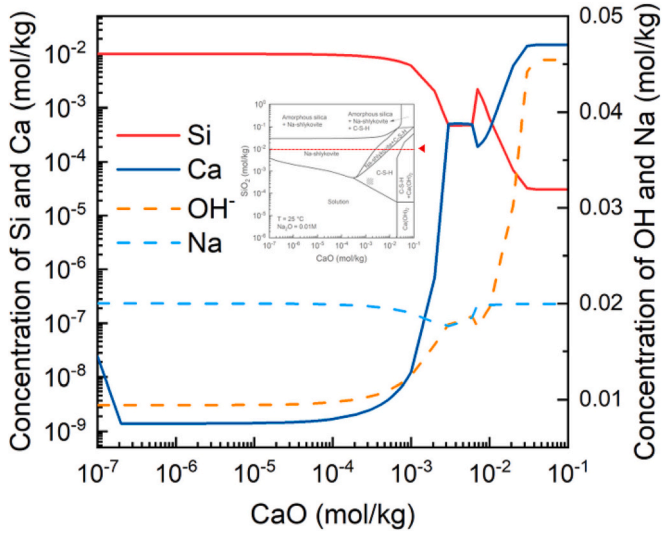

Fig. 6. The concentrations of Si, Ca, Na, and OH^- in the aqueous solution with increasing addition of CaO, with fixed 0.01 mol/kg of SiO_2 and 0.01 mol/kg of Na_2O (indicated on the inset as a line sketched across a copy of Fig. 3a, for context).

In order to investigate the difference of solution chemistries at different concentrations of SiO_2 with the increase of the concentration of Na_2O, three concentrations of SiO_2 are chosen for further analysis of the aqueous phase, and marked as red dashed lines on the inset phase diagrams in Figs. 7 and 8.

At the lower concentration of SiO_2 selected (10^{-6} mol/kg, Fig. 7a), the red line falls across two compositional regions, and the calculated component molalities are in good agreement with the phase diagram. The concentration of Ca reaches a plateau before the concentration of Na_2O reaches 0.02 mol/kg because there is no solid phase formed, meaning that all dissolved ions are in the solution. With an increase in Na_2O, $Ca(OH)_2$ starts to form, which leads to the decrease of the concentration of Ca to maintain saturation in the aqueous phase. Since no Na-containing phase is formed at 10^{-6} mol/kg of SiO_2, the concentration of dissolved Na ions gradually increases.

When the concentration of SiO_2 reaches 0.01 mol/kg (Fig. 7b), C-S-H is the only solid phase identified in the whole range of Na_2O addition levels. Therefore, the concentrations of Ca are at very low and constant. Due to the low concentration of CaO, the rest of the Si remains in the solution when the amount of formation of C-S-H reaches the maximum possible level. Also, Na-shlykovite is not found across most of this compositional range, meaning that there is no incorporation of Na into solid phases, and thus the trend in Na concentration is similar to that at low concentration of SiO_2.

Moving to higher Si concentration, Na-shlykovite appears at 2 mol/kg of SiO_2 (Fig. 8), and the trends for the four components are different compared with the two lower concentrations that were discussed above. Due to the formation of Na-shlykovite, the amount of Ca reduces in the very low Na_2O concentration range. In addition, the increment in dissolved Na concentration becomes very slight because of the formation of the ASR product. The concentration of SiO_2 is sufficient to form the ASR product by consuming Na and Ca, and amorphous silica can also form. However, the amount of amorphous silica declines with an increased concentration of Na_2O added, as the rising pH also increases SiO_2 solubility. Therefore, the molarities of Si in the solution become large. When the concentration of Na_2O reaches 0.47 mol/kg, C-S-H and Na-shlykovite co-exist in the phase diagram and the concentration of Si in the solution stays constant then reduces above this addition level, as the supplied Si starts to react with Na_2O and CaO to form various constituents of the C-S-H solid solution. Also, less Ca is consumed by the reaction, thus causing an increase in the amount of Ca in the solution.

Shi et al. [22,29,30] have presented some thermodynamic modelling to check their experimental data for ASR processes at 80 °C. In this work, we have refined and extended their results and apply this to the analysis of reaction at 25 °C. The results have some similarities. For example, ASR products are stable at certain concentrations of alkali ions, where they convert to C-S-H when increasing the concentration of dissolved alkalis and Ca [29]. However, the specific point of conversion of ASR products to C-S-H (or vice versa) is unclear in those previous studies. This work provides more comprehensive modelling data that might guide experiments, and aid in more accurately defining and understanding the existence of a 'pessimum' content of alkalis. More importantly, the modelling presented in this paper is extended to ambient temperature. It means that these results have the possibility to be used in predicting alkali-silica reaction under realistic field conditions. Finally, this work may indicate the need to carefully consider the choice of alkali content in the standard tests for ASR, to gain optimised experimental data and avoid the possibility of false negative test results.

4. Conclusions

The aim of this study has been to estimate the thermodynamic parameters for Na- and K-shlykovite phases that are sometimes found to form in concrete due to alkali-silica reaction (ASR) at ambient temperatures. We refined solubility products of these two ASR products by

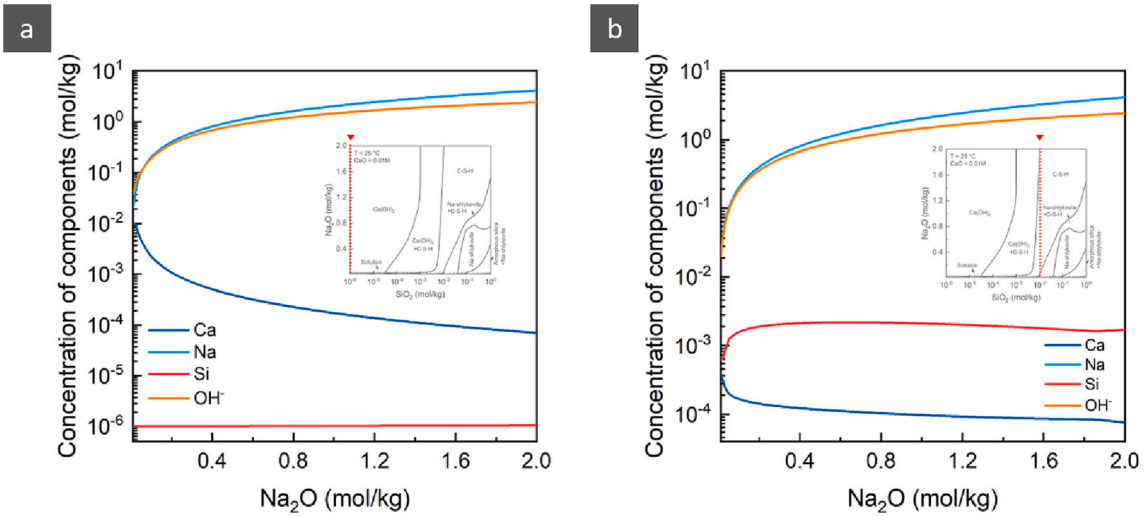

Fig. 7. The concentrations of Si, Ca, Na, and OH^- in the solution with increased addition of Na_2O. a: 10^{-6} mol/kg of SiO_2, b: 0.01 mol/kg of SiO_2. The inset diagram in each case places this calculation with respect to the phase diagram by reproducing Fig. 4a, with a dashed line to indicate the compositions depicted.

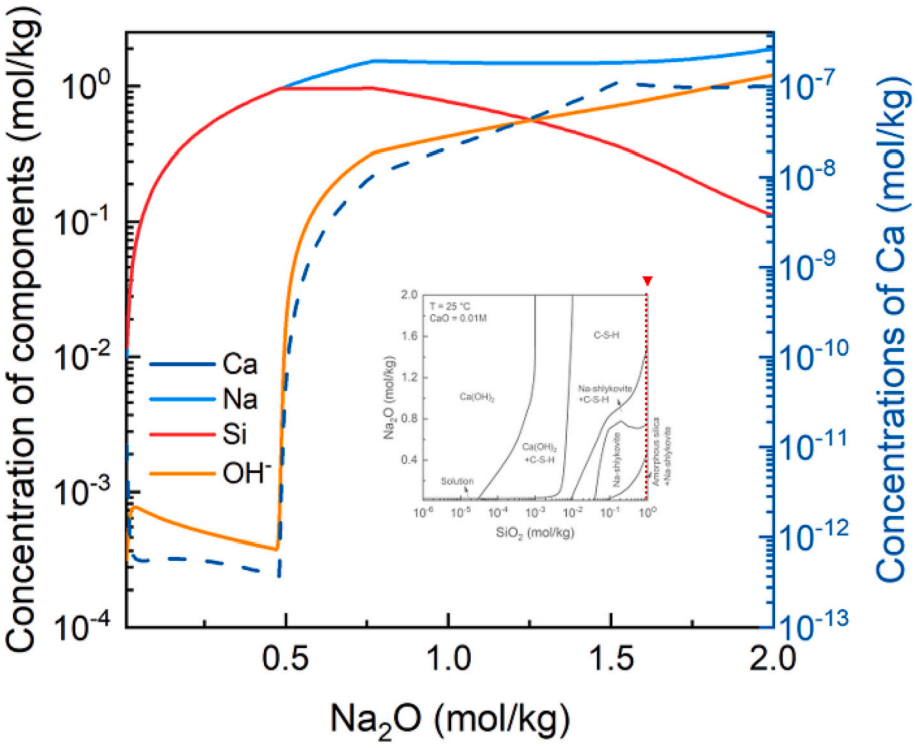

Fig. 8. The concentrations of Si, Na, and OH^- (left-hand axis, solid lines), and Ca (right-hand axis, dashed line) present in the solution as a function of the concentration of Na_2O added, with 1 mol/kg of SiO_2. The inset diagram places this calculation with respect to the phase diagram by reproducing Fig. 4a, with a dashed line to indicate the compositions depicted.

recalculating pH values reported in earlier studies, using the GEM-Selektor v.3 software. Thermodynamic modelling is used to predict the formation of these two shlykovite phases in $(Na,K)_2O$-CaO–SiO_2-H_2O system, using GEMS with the Cemdata18 database and new thermodynamic parameters obtained from the current study. Binary phase diagrams with different concentration of alkalis are established to verify the reliability of database and compare with experimental data that has been published. The conclusions are summarised as follows:

(1) Without alkali ions there is no ASR product found in the binary phase diagram. When adding 0.01 mol/kg of Na_2O, Na-shlykovite is found, and regions that form this ASR product occupy areas that formed C-S-H and amorphous silica in the absence of Na. The ASR product can co-exist with C-S-H, which indicates that with an increased concentration of CaO, Na has been partially consumed via the formation of ASR products, while the rest of the Ca continues to react with amorphous silica to form C-S-H.

(2) Adding more Na does not always mean the formation of more Na-shlykovite. There is a maximum concentration of Na_2O that enables the formation of Na-shlykovite. Below 1.48 mol/kg of Na_2O, the existence of ASR product proves the possibility of alkali-silica reaction happening. However, beyond that

concentration, this type of ASR products is no longer predicted to form, due to the suppression of calcium solubility.

(3) Solubility results show that adding more Na_2O increases the pH of solution, thus increasing the dissolution of Si and further forming more Na-shlykovite. The formation of Na-shlykovite consumes Ca and Na in the solution, which leads to the decrease in the concentration of Ca and Na. Less Ca is used to take part in the reaction due to the suppression of calcium solubility, and the Si source starts to react with Na_2O and CaO to form C-S-H instead of shlykovite-group minerals.

CRediT authorship contribution statement

Haoliang Jin: Conceptualization, Investigation, Methodology, Writing – original draft, Writing – review & editing. **Sam Ghazizadeh:** Investigation, Methodology, Writing – review & editing. **John L. Provis:** Investigation, Writing – review & editing.

Declaration of competing interest

The authors declare that they have no known competing financial interests or personal relationships that could have appeared to influence the work reported in this paper.

Data availability

Data will be made available on request.

Acknowledgement

This research did not receive any specific grant from funding agencies in the public, commercial, or not-for-profit sectors.

Appendix

Table A1
The crystallographic parameters of K-shlykovite and Na-shlykovite according to the analysis of natural mineral specimens [16], and from molecular simulation results [31].

ASR products	K-shlykovite	Na-shlykovite
Chemical composition	$KCaSi_4O_8(OH)_3 \cdot 2H_2O$	$NaCaSi_4O_8(OH)_3 \cdot 2.3H_2O$
Crystal system	Monoclinic	
a[Å]	6.4897	6.35
b[Å]	6.9969	6.92
c[Å]	26.714	24.89
β[°]	94.597	89.9
V[$Å^3$]	1209.12	1089

Table A2
Thermodynamic data for phases and species used in the modelling, collected from Cemdata18.1 [23].

Phase	V° (cm^3/mol)	$\Delta_f H°$ (kJ/mol)	$\Delta_f G°$ (kJ/mol)	S° (J/mol·K)	Cp° (J/mol·K)
C-S-H (CSHQ solid solution)					
TobH, $C_{2/3}SH_{1.5}$	55	−1841.5	−1668.56	89.9	141.6
TobD, $C_{5/6}S_{2/3}H_{1.83}$	45	−1742.4	−1570. 89	121.8	166.9
JenH, $C_{1.33}SH_{2.17}$	76	−2506.3	−2273.99	142.5	207.9
JenD, $C_{1.5}S_{0.67}H_{2.5}$	81	−2400.7	−2169.56	173.4	232.8
NaSH, $N_{0.5}S_{0.2}H_{0.45}$	10.5	−478	−431.2	41.2	37.9
KSH, $K_{0.5}S_{0.2}H_{0.45}$	12.4	−489.6	−440.8	48.4	40.6
Portlandite, $Ca(OH)_2$	33.1	−985	−897	83.4	87.5
SiO_2 (amorphous)	29	−903	−849	41.3	44.5

Species	V° (cm^3/mol)	$\Delta_f H°$ (kJ/mol)	$\Delta_f G°$ (kJ/mol)	S° (J/mol·K)	Cp° (J/mol·K)
Ca^{2+}	−18.4	−543.1	−552.8	−56.5	−30.9
$CaOH^+$	5.8	−751.6	−717	28	6.0
$CaHSiO_3^+$ ($+ H_2O = CaSiO(OH)_3^+$)	−6.7	−1687	−1574	−8.3	137.8
$CaSiO_3$ ($+ H_2O = CaSiO_2(OH)_2$)	15.7	−1668	−1518	−136.7	88.9
K^+	9.0	−252.1	−282.5	101	8.4
KOH	15	−474.1	−437.1	108.4	−85
Na^+	−1.2	−240.3	−261.9	58.4	38.1
NaOH	3.5	−470.1	−418.1	44.8	−13.4
$HSiO_3^-$ ($+ H_2O = SiO(OH)_3^-$)	4.5	−1145	−1014	20.9	−87.2
SiO_2 ($+ 2H_2O = Si(OH)_4$)	16.1	−887.9	−833.4	41.3	44.5
SiO_3^{2-} ($+ H_2O = SiO_2(OH)_2^{2-}$)	34.1	−1099	−938.5	−80.2	119.8
$Si_4O_{10}^{4-}$	100.4	−3916	−3600.8	305.2	328.6
OH^-	−4.7	−230	−157.3	−10.7	−136.3
H^+	0	0	0	0	0

(continued on next page)

Table A2 (*continued*)

Phase	V° (cm^3/mol)	$\Delta_f H°$ (kJ/mol)	$\Delta_f G°$ (kJ/mol)	S° (J/mol·K)	Cp° (J/mol·K)
H_2O	18.1	−285.9	−237.2	69.9	75.4
O_2	30.5	−12.2	16.4	109	234.1

References

[1] E. Boehm-Courjault, S. Barbotin, A. Leemann, K. Scrivener, Microstructure, crystallinity and composition of alkali-silica reaction products in concrete determined by transmission electron microscopy, Cem. Concr. Res. 130 (2020), 105988, https://doi.org/10.1016/j.cemconres.2020.105988.

[2] H. Maraghechi, F. Rajabipour, C.G. Pantano, W.D. Burgos, Effect of calcium on dissolution and precipitation reactions of amorphous silica at high alkalinity, Cem. Concr. Res. 87 (2016) 1–13, https://doi.org/10.1016/j.cemconres.2016.05.004.

[3] C. Balachandran, J.F. Muñoz, T. Arnold, Characterization of alkali silica reaction gels using Raman spectroscopy, Cem. Concr. Res. 92 (2017) 66–74, https://doi.org/10.1016/j.cemconres.2016.11.018.

[4] A. Leemann, Raman microscopy of alkali-silica reaction (ASR) products formed in concrete, Cem. Concr. Res. 102 (2017) 41–47, https://doi.org/10.1016/j.cemconres.2017.08.014.

[5] A. Leemann, Z. Shi, J. Lindgård, Characterization of amorphous and crystalline ASR products formed in concrete aggregates, Cem. Concr. Res. 137 (2020), 106190, https://doi.org/10.1016/j.cemconres.2020.106190.

[6] G. Geng, et al., An in-situ 3D micro-XRD investigation of water uptake by alkali-silica-reaction (ASR) product, Cem. Concr. Res. 141 (2021), https://doi.org/10.1016/j.cemconres.2020.106331.

[7] G. Geng, et al., Atomistic structure of alkali-silica reaction products refined from X-ray diffraction and micro X-ray absorption data, Cem. Concr. Res. 129 (2020), 105958, https://doi.org/10.1016/j.cemconres.2019.105958.

[8] Z. Shi, C. Shi, R. Zhao, S. Wan, Comparison of alkali-silica reactions in alkali-activated slag and Portland cement mortars, Mater. Struct. 48 (2015) 743–751, https://doi.org/10.1617/s11527-015-0535-4.

[9] Z. Shi, C. Shi, J. Zhang, S. Wan, Z. Zhang, Z. Ou, Alkali-silica reaction in waterglass-activated slag mortars incorporating fly ash and metakaolin, Cem. Concr. Res. 108 (2018) 10–19, https://doi.org/10.1016/j.cemconres.2018.03.002.

[10] A. Fernández-Jiménez, F. Puertas, The alkali-silica reaction in alkali-activated granulated slag mortars with reactive aggregate, Cem. Concr. Res. 32 (7) (2002) 1019–1024, https://doi.org/10.1016/S0008-8846(01)00745-1.

[11] A. Leemann, T. Katayama, I. Fernandes, M.A.T.M. Broekmans, Types of alkali-aggregate reactions and the products formed, Proc. Inst. Civ. Eng.: Constr. Mater. 169 (3) (2016) 128–135, https://doi.org/10.1680/jcoma.15.00059.

[12] K. Peterson, D. Gress, T. Van Dam, L. Sutter, Crystallized alkali-silica gel in concrete from the late 1890s, Cem. Concr. Res. 36 (8) (2006) 1523–1532, https://doi.org/10.1016/j.cemconres.2006.05.017.

[13] Y. Kawabata, K. Yamada, The mechanism of limited inhibition by fly ash on expansion due to alkali–silica reaction at the pessimum proportion, Cem. Concr. Res. 92 (2017) 1–15, https://doi.org/10.1016/j.cemconres.2016.11.002.

[14] W.F. Cole, C.J. Lancucki, Products formed in an aged concrete the occurrence of okenite, Cem. Concr. Res. 13 (5) (1983) 611–618, https://doi.org/10.1016/0008-8846(83)90049-2.

[15] Z. Shi, G. Geng, A. Leemann, B. Lothenbach, Synthesis, characterization, and water uptake property of alkali-silica reaction products, Cem. Concr. Res. 121 (January) (2019) 58–71, https://doi.org/10.1016/j.cemconres.2019.04.009.

[16] I.V. Pekov, et al., Shlykovite KCa[Si_4O_9(OH)]·3H_2O and cryptophyllite K_2Ca[Si_4O_{10}]·5H_2O, new mineral species from the Khibiny alkaline pluton, Kola peninsula, Russia, Geol. Ore Depos. 52 (8) (2010) 767–777, https://doi.org/10.1134/S1075701510080088.

[17] R. Dron, F. Brivot, Thermodynamic and kinetic approach to the alkali-silica reaction. Part 2: experiment, Cem. Concr. Res. 23 (1) (1993) 93–103, https://doi.org/10.1016/0008-8846(92)90118-F.

[18] R. Dron, F. Brivot, Thermodynamic and kinetic approach to the ASR part 1 - concepts, Cem. Concr. Res. 22 (1992) 941–948.

[19] T. Kim, J. Olek, Chemical sequence and kinetics of alkali-silica reaction part II. A thermodynamic model, J. Am. Ceram. Soc. 97 (7) (2014) 2204–2212, https://doi.org/10.1111/jace.12830.

[20] G.D. Guthrie, J.W. Carey, A thermodynamic and kinetic model for paste-aggregate interactions and the alkali-silica reaction, Cem. Concr. Res. 76 (2015) 107–120, https://doi.org/10.1016/j.cemconres.2015.05.004.

[21] X. Hou, L.J. Struble, R.J. Kirkpatrick, Formation of ASR gel and the roles of C-S-H and portlandite, Cem. Concr. Res. 34 (9) (2004) 1683–1696, https://doi.org/10.1016/j.cemconres.2004.03.026.

[22] Z. Shi, B. Lothenbach, The role of calcium on the formation of alkali-silica reaction products, Cem. Concr. Res. 126 (2019), 105898, https://doi.org/10.1016/j.cemconres.2019.105898.

[23] B. Lothenbach, et al., Cemdata18: a chemical thermodynamic database for hydrated Portland cements and alkali-activated materials, Cem. Concr. Res. 115 (2019) 472–506, https://doi.org/10.1016/j.cemconres.2018.04.018.

[24] Z. Shi, A. Leemann, D. Rentsch, B. Lothenbach, Synthesis of alkali-silica reaction product structurally identical to that formed in field concrete, Mater. Des. 190 (2020), 108562, https://doi.org/10.1016/j.matdes.2020.108562.

[25] S. Ghazizadeh, T. Hanein, J.L. Provis, T. Matschei, Estimation of standard molar entropy of cement hydrates and clinker minerals, Cem. Concr. Res. 136 (2020), 106188, https://doi.org/10.1016/j.cemconres.2020.106188.

[26] L. Glasser, H.D.B. Jenkins, Ambient isobaric heat capacities, $C_{p,m}$, for ionic solids and liquids: an application of volume-based thermodynamics (VBT), Inorg. Chem. 50 (2011) 8565–8569.

[27] P.W. Brown, The system Na_2O-CaO-SiO_2-H_2O, J. Am. Ceram. Soc. 61 (6) (1990) 3457–3461.

[28] F. Winnefeld, et al., RILEM TC 247-DTA round robin test: sulfate resistance, alkali-silica reaction and freeze–thaw resistance of alkali-activated concretes, Mater. Struct. 53 (2020), 140, https://doi.org/10.1617/s11527-020-01562-0.

[29] Z. Shi, B. Lothenbach, The combined effect of potassium, sodium and calcium on the formation of alkali-silica reaction products, Cem. Concr. Res. 127 (2020), 105914, https://doi.org/10.1016/j.cemconres.2019.105914.

[30] Z. Shi, B. Ma, B. Lothenbach, Effect of Al on the formation and structure of alkali-silica reaction products, Cem. Concr. Res. 140 (2021), 106311, https://doi.org/10.1016/j.cemconres.2020.106311.

[31] T. Honorio, O.M. Chemgne Tamouya, Z. Shi, A. Bourdot, Intermolecular interactions of nanocrystalline alkali-silica reaction products under sorption, Cem. Concr. Res. 136 (2020), 106155, https://doi.org/10.1016/j.cemconres.2020.106155.

Update

Cement and Concrete Research
Volume 176, Issue , February 2024, Page

DOI: https://doi.org/10.1016/j.cemconres.2023.107405

Cement and Concrete Research 176 (2024) 107405

Contents lists available at ScienceDirect

Cement and Concrete Research

journal homepage: www.elsevier.com/locate/cemconres

Corrigendum

Corrigendum to "Assessment of the thermodynamics of Na,K-shlykovite as potential alkali-silica reaction products in the $(Na,K)_2O$-CaO–SiO_2-H_2O system" [Cement and Concrete Research (2023), 172, #107253]

Haoliang Jin [a], Sam Ghazizadeh [b], John L. Provis [a,*]

[a] Department of Materials Science and Engineering, The University of Sheffield, United Kingdom
[b] Special Services, Mott MacDonald, London, United Kingdom

The authors regret that an error was made in compiling Table 1 of our paper [1] concerning the $\Delta_f H$ of K-shlykovite and Na-shlykovite. The correct $\Delta_f H$ of the K-shlykovite and Na-shlykovite are -5163.6 ± 8 kJ/mol for K-shlykovite and -5267.5 ± 9 kJ/mol for Na-shlykovite, respectively, as detailed in the Table below.

The authors would like to apologise for any inconvenience caused and would like to highlight that the wrong parameters did not affect the calculations presented in the paper, as the correct values had been used throughout.

Declaration of competing interest

The authors declare that they have no known competing financial interests or personal relationships that could have appeared to influence the work reported in this paper.

Table 1
Thermodynamic properties for ASR products at 25 °C.

Products	V° (cm^3/mol)	V_m (nm^3·formula-$unit^{-1}$)	$\Delta_f H^\circ$ (kJ/mol)*	$\Delta_f G^\circ$ (kJ/mol)*	S° (J/mol·K)*	Cp° (J/mol·K)*	$\log_{10}K$ at 25 °C
K-shlykovite: $KCaSi_4O_8(OH)_3{\cdot}2H_2O$	183	0.3	-5163.6 ± 8	-5293.1 ± 3	485.8 ± 48	426.4 ± 42	-31.2 ± 1.2
Na-shlykovite: $NaCaSi_4O_8(OH)_3{\cdot}2.3H_2O$	164	0.27	-5267.5 ± 9	-5364.4 ± 2	435.9 ± 43	382.5 ± 38	$-34.0.8 \pm 0.4$

* The uncertainties in entropy and heat capacity here were estimated to be ±10 %, which were propagated also to give the uncertainties in enthalpy and Gibbs free energy.

DOI of original article: https://doi.org/10.1016/j.cemconres.2023.107253.
* Corresponding author.
E-mail addresses: hjin15@sheffield.ac.uk (H. Jin), sam.ghazizadeh@mottmac.com (S. Ghazizadeh), j.provis@sheffield.ac.uk (J.L. Provis).

https://doi.org/10.1016/j.cemconres.2023.107405

Available online 14 December 2023

Acknowledgement

The authors are grateful to Dr. Hans Meeussen for bringing this issue to our attention, and for constructive discussions that enabled us to isolate and fix the error.

References

[1] H. Jin, S. Ghazizadeh, J.L. Provis, Assessment of the thermodynamics of Na,K-shlykovite as potential alkali-silica reaction products in the $(Na,K)_2O$-CaO–SiO_2-H_2O system, Cem. Concr. Res. 172 (2023), 107253, https://doi.org/10.1016/j.cemconres.2023.107253.